

Image processing Master project : Reconstructing the Cosmic
Microwave Background from Planck maps

Massonneau Warren, Mercier Wilfried

21 mars 2019

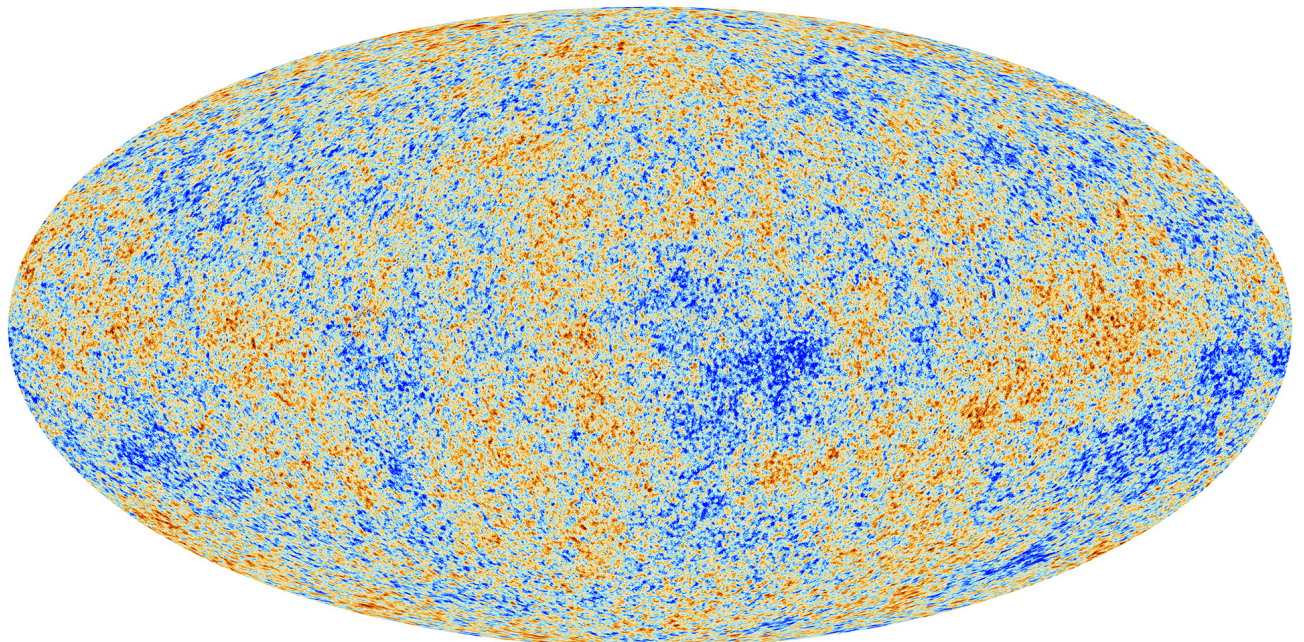


FIGURE 1 – Map of the Cosmic Microwave Background [Planck 2013]

1 Introduction

The Planck mission was launched in 2009 and revealed its first results in 2013. Its main objective was to measure with a better accuracy the Cosmic Microwave Background (CMB) within the microwave spectral range (of the order of 10²GHz) reflecting the structure of the primordial Universe. The transmitted data from the satellite were given in many frequency domains (HFI maps centred at 100, 143, 217, 353, 545 and 857GHz). These frequencies were chosen among others for their capability to isolate secondary components adding up to the CMB. Indeed, raw data unfortunately do not allow us to see this fossil radiation. Secondary sources, such as galactic dust (which emits in the far infrared and which dominates in higher frequency maps) or SZ sources (inverse Compton scattering of the photons going through the hot gas within galaxy clusters).

In order to extract and analyse a map containing only the CMB component, we need to use a technique which will identify the CMB signal within the different maps and which will eliminate the other components. That is what we have done during this master project by using an Internal Linear Combination (ILC) technique on HFI Planck maps^a. This method tries to find the best linear combination between the frequency maps by minimising our final map variance.

In Section 2, we describe the modifications we had to make to the maps before their treatment. In Sections 3 and 4, we describe the two ILC methods we used, and then we briefly compare their results. A theoretical description of the power spectrum analysis performed during this project, as well as the final power spectrum we obtained are given in Sections 5, and 6. We compare our power spectrum to that of Planck as well as the best fit parameters between our spectrum and the theoretical one obtained with the *Classy* code in Section 7. Finally, we briefly conclude on the work performed during this project and the possible openings.

2 Treatment of Planck maps

2.1 Uniforming unities

The Planck maps we used for this work were not all given in the same unit because of two different calibrations (see [7], Section 3.2). The maps within the range [100 – 353]GHz were calibrated on the CMB dipole and are given in K_{CMB} unit (Kelvin unit normalised by the mean contribution at 2.725K), when the 545 et 857GHz maps were calibrated on the emission of some planetary and galactic sources and are given in MJy.sr⁻¹.

In order to work on the maps, the first step was to convert them all in the same unit. We chose, for sake of simplicity in the following analysis, to convert the two highest frequency maps in K_{CMB} unit^b.

2.2 Dealing with beam smearing and pixellisation

The six HFI Planck maps underwent a smearing of their information below a given size because of the Point Spread Function (PSF) of the instrument. Nevertheless, it is not the same for all frequencies, and it is thus important to correct this effect before working on the maps. If we note D_i the Planck map at the frequency i and ψ the PSF, then we can model its effect on the maps by a convolution $D_i * \psi$.

In addition to that, we also need to take into account the equivalent effect (but at even lower scale lengths) of the pixellisation of the maps which will average any information within each pixel (see [8], Appendix F for more details). If we note P this effect, the the Planck maps can be written as

$$M_i = D_i * \psi * P \quad (1)$$

The PSF can be modelled in first approximation by a Gaussian function (see [8], Appendix B) with a null mean and a non-zero Full Width at Half Maximum (FWHM) or equivalently a variance which will change with frequency. The values of the FWHM for each map are given in Table 3 of [8].

Every information within a scale-length lower than the FWHM are smoothed, which means that the most physically useful information are contained within scales larger than $FWHM_{\max} = \max(FWHM)$. It is thus necessary to correct any other map for which the FWHM is lower, i.e. we want

$$FWHM \rightarrow FWHM_{\max} \quad (2)$$

Since all PSFs are approximated by Gaussians as said earlier, this implies the following relation

$$FWHM_{\max}^2 = FWHM^2 + FWHM_{\text{corr}}^2 \quad (3)$$

a. We used both the full mission maps and the half-mission ones

b. It is advised in [7] to make the inverse conversion because the one we use will give more weight to the lower frequency of the filters at 545 and 857GHz (see Fig. 14 in the same paper). This can lead in an amplification of already present errors.

where $FWHM_{\text{corr}}$ is the correction to give in order for Eq. 2 to be correct. The highest FWHM ($9.66'$) being for the 100GHz map, we need to convolve all the other maps by a Gaussian function $\mathcal{G}(0, FWHM_{\text{corr}}^2 = (9.66')^2 - FWHM^2)$.

3 Reconstructing the CMB by ILC

3.1 The ILC method

The standard method for the ILC tells us that all the available maps ($N_{\text{obs}} = 6$ in total, all indexed with i in Eq. 4) can be written for the pixel p as

$$x_i(p) = a_i s(p) + n_i(p) \quad (4)$$

which we can rewrite as

$$\mathbf{x}(p) = \mathbf{a}s(p) + \mathbf{n}(p) \quad (5)$$

where $\mathbf{x}(p)$ and $\mathbf{n}(p)$ are respectively the total emission and noise vectors, for all of the N_{obs} frequencies. The matrix \mathbf{a} corresponds to a mixing matrix which involves spectral dependant parameters for each astrophysical component (CMB, SZ (Sunyaev-Zel'dovich)) as well as the spectral response of the i^{th} frequency. Finally, $s(p)$ is the map in which we are interested, namely the CMB component.

The objective is then to find an estimator \hat{s}_{ILC} (a new map) for which the variance will be minimised. We retrieve it by using a linear combination between our weights \mathbf{w}^t and our total emission map $\mathbf{x}(p)$ in order to only keep the CMB component [1]. The weights \mathbf{w}^t can be analytically calculated (see [3]) so that we get a new map \hat{s}_{ILC} given by

$$\hat{s}_{\text{ILC}} = \frac{\mathbf{a}^t \mathcal{C}_s^{-1} \mathbf{x}}{\mathbf{a}^t \mathcal{C}_s^{-1} \mathbf{a}} \quad (6)$$

where \mathcal{C}_s is the co-variance matrix of all the maps.

3.2 ILC with one component

For an ILC with only one component (the CMB) we chose $\mathbf{a} = (1, 1, 1, 1, 1, 1)^t$. Then, we get our first CMB map from the 6 frequency maps.

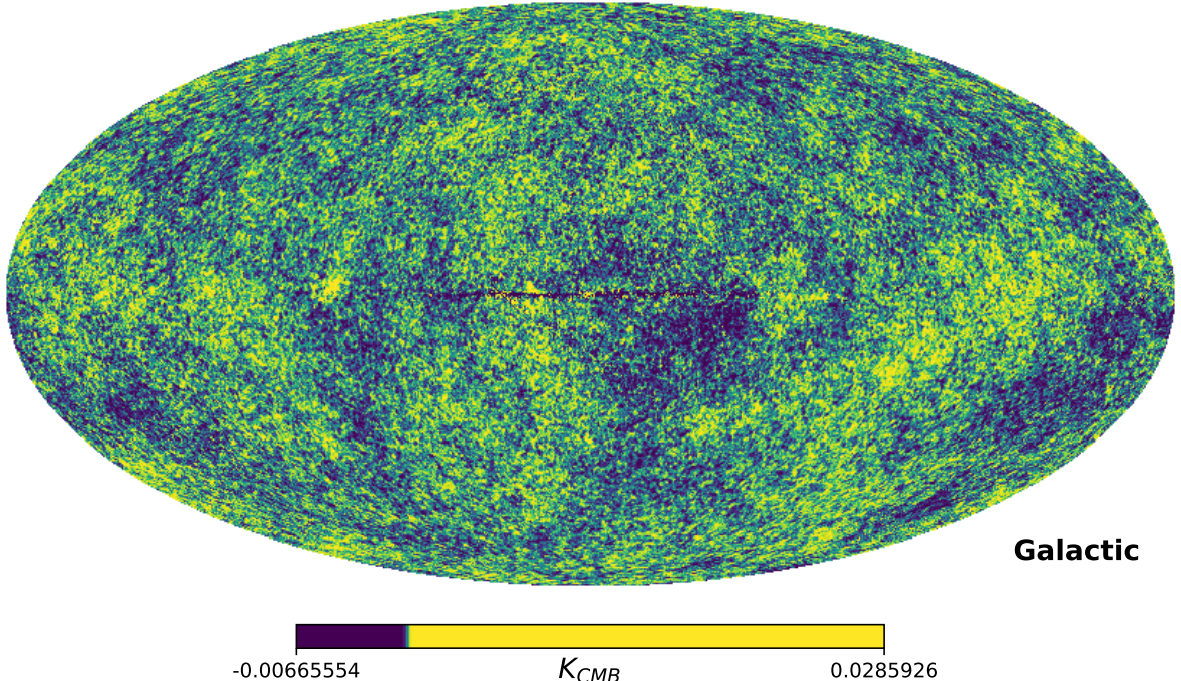


FIGURE 2 – CMB with a one-component ILC

We can see that the map has a thin strip towards the galactic plane. This is a residual the ILC did not manage to take off due to the strong presence of the galactic component at high frequencies. Better results will be available in Section 4.1.

Frequency (GHz)	100	143	217	353	545	857
Weight	-0.79	1.09	0.93	-0.24	$5.58 \cdot 10^{-3}$	$-3.62 \cdot 10^{-6}$

TABLE 1 – Weight table obtained for a one-component ILC method.

To get and idea if our map matches the CMB signal, we could compare our weights (given in Table 1) with those given by the Planck Collaboration. Unfortunately, we did not manage to find them in due time. Thus we interpret our weights as follows : the galactic plane is dominated by dust, which we see mainly at high frequencies (in the 545 and 857 GHz maps, as well as slightly in the 353GHz). This adds up to the SZ component, which is mainly within the 143 and 353GHz maps. The CMB component, which is present on every map, is therefore poorly visible on high frequency ones. Thus, we expect our weights on those maps to reduce their impact in the linear combination.

By comparing our prediction with Table 1, we can see that the low frequency weights are (in absolute value) close to unity, whereas high frequency ones are much closer to 0.

3.3 ILC with two components

Performing an ILC with only one component is insufficient in the sens that nothing prevents the other components such as SZ to disappear from the final map. Moreover, it is possible to remove another component (we will choose SZ in the following) analytically by using a new estimator as well as better adjusted weights (Eq. 8). Indeed, if we split our signal in the same manner

$$\mathbf{x}(p) = \mathbf{a}s(p) + \mathbf{b}y(p) + \mathbf{n}(p) \quad (7)$$

and if we constrain the thermal SZ component ($y(p)$) to be zero (which is the same as $\mathbf{w}^t \mathbf{b} = 0$), we get the following weights (see [9])

$$\mathbf{w}^t = \frac{(\mathbf{b}^t \mathcal{C}_{s,r}^{-1} \mathbf{b}) \mathbf{a}^t \mathcal{C}_{s,r}^{-1} - (\mathbf{a}^t \mathcal{C}_{s,r}^{-1} \mathbf{b}) \mathbf{b}^t \mathcal{C}_{s,r}^{-1}}{(\mathbf{a}^t \mathcal{C}_{s,r}^{-1} \mathbf{a})(\mathbf{b}^t \mathcal{C}_{s,r}^{-1} \mathbf{b}) - (\mathbf{a}^t \mathcal{C}_{s,r}^{-1} \mathbf{b})^2} \quad (8)$$

And we get a new map, but this time with the SZ component constrained.

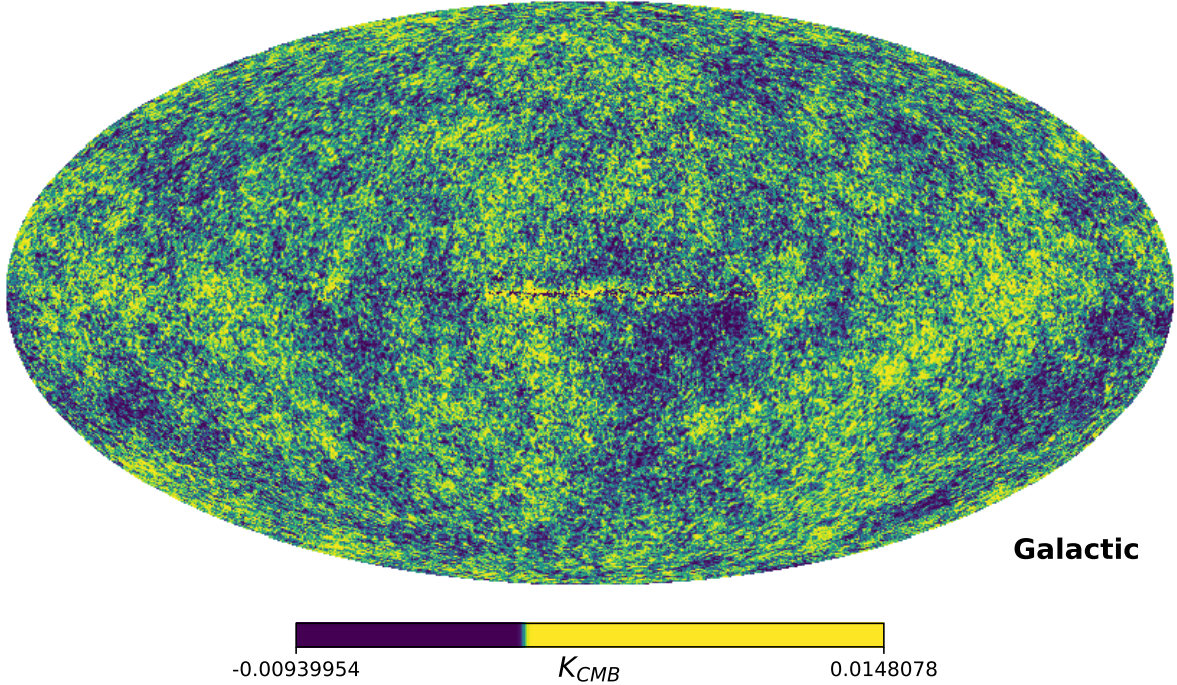


FIGURE 3 – CMB with a two-component ILC (constrained SZ).

Frequency (en GHz)	100	143	217	353	545	857
Weight	-0.98	1.03	1.17	-0.22	$4.59 \cdot 10^{-4}$	$2.52 \cdot 10^{-5}$

TABLE 2 – Weights table with a two-component ILC method.

We can notice that the weights given in Table 2 are quite close to those in Table 1. Thus, they cannot help us to compare the two methods (constrained and unconstrained ILC) in order to know which one is better than the other.

Indeed, at first sight, apart from the galactic strip being slightly less pronounced in the constrained ILC, it is hard to see any difference between Figures 2 and 3.

In order to know if the two-components ILC gives us a better result, we look at places where the SZ signal is present in the map obtained with the first method but not in the map from the second one : galaxy clusters. With the help of the P3 group, who were working on sky patches with only SZ signal, we went looking for Coma and Abell 2162 clusters on our maps. When we computed the residual between our maps from the two methods (difference between the maps around both clusters). We should see those clusters appear if the constrained ILC method did work correctly. That is what we observe, as is shown in Figure 4.

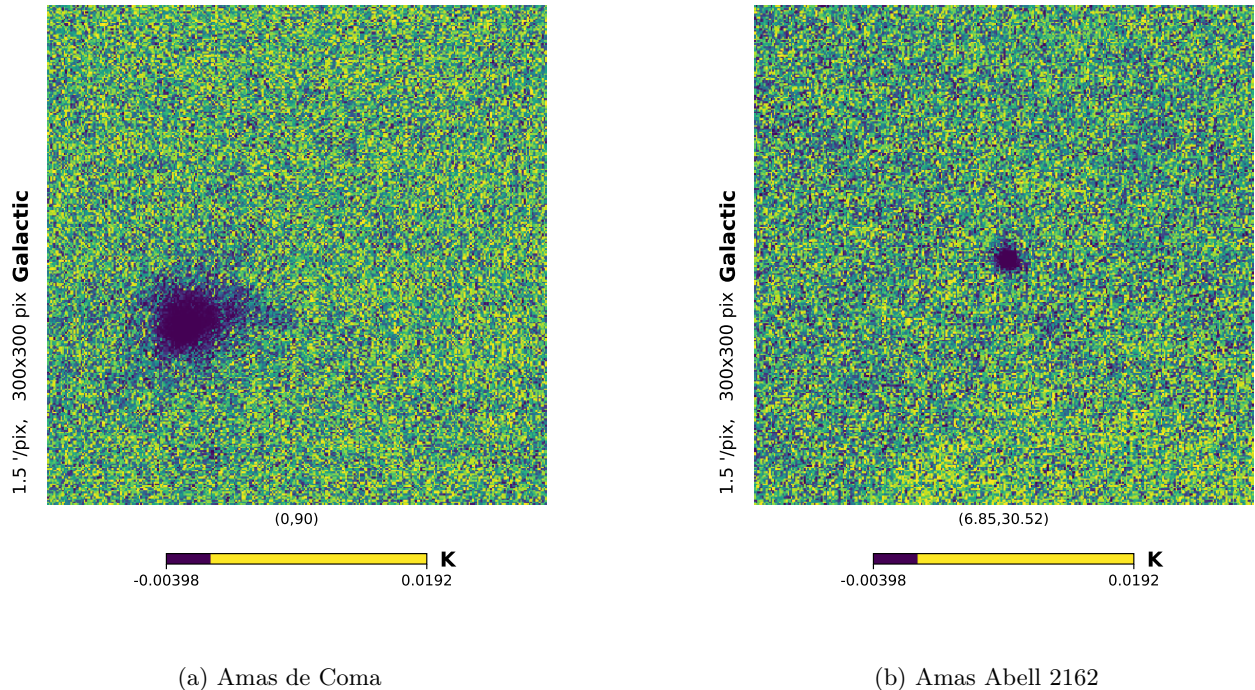


FIGURE 4 – Two galaxy clusters appear in our maps when we compute the residual between the two ILC methods.

We can then conclude that the two ILC methods did work correctly, but this does not tell us anything about which one is the best. In order to know if our signal within our maps is really the CMB or something else, we need to compute and look at the power spectrum of both maps. This is what is done in Section 5.

By lack of time, in the following sections, we focused on the one-component ILC method only.

4 Improving the ILC

4.1 Masked maps

In order to not take into account the galactic plane which is dominated at high frequencies by dust and, as we saw, since it is not completely eliminated by the ILC, we decided to work on masked maps.

The objective was to hide a part of the sky (preferentially the galactic plane) by choosing an arbitrary maximum temperature beyond which we hid the pixels. We adjusted this value based on the typical temperature within the galactique plan (this region being the hottest in the 857GHz), and we varied it according to the proportion of the galactic plane we wanted to hide.

The mask computed at 857GHz was used in every map, in such a way that it does not bring any more difficulty when performing the ILC.

Therefore, we only worked with the one-component ILC and a mask hiding between 10% and 45% of the full sky, with steps of 5% (see Fig. 6). The comparison between the theoretical CMB and our results suggests that it is preferable to use a mask hiding between 15 and 20% of the sky.

Thus, in the following sections, we chose to always use a mask hiding about 20% of the galactic plane. An example is given in Fig. 5.

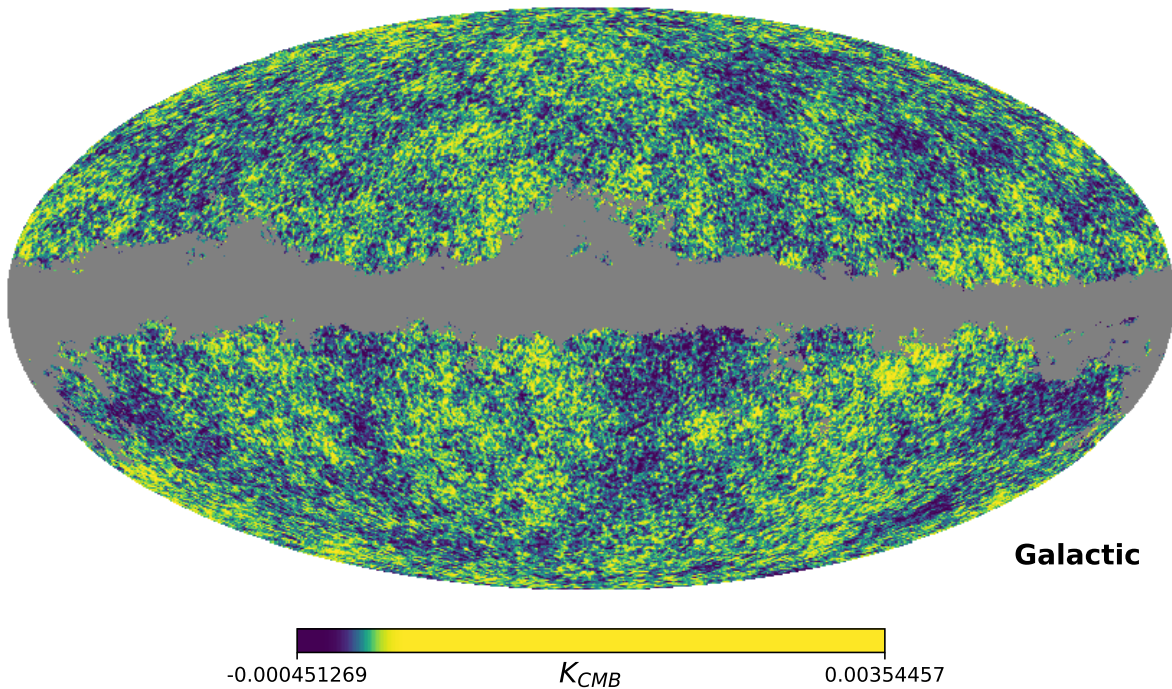


FIGURE 5 – Example of a mask hiding roughly 20% of the sky. The one-component ILC was performed on the unmasked areas only to reduce the impact of galactic dust in the final power spectrum.

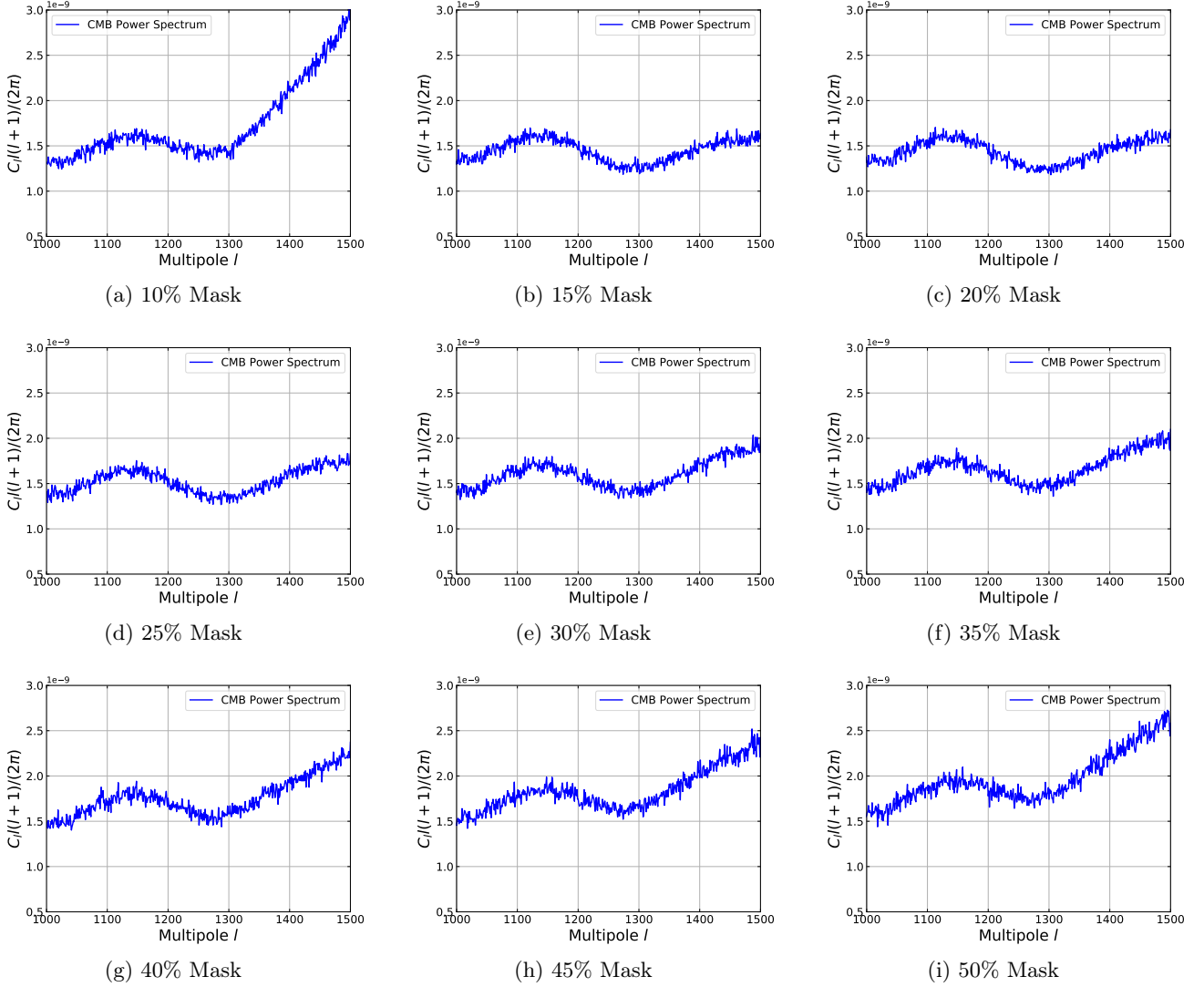


FIGURE 6 – Zoom on the 4th and 5th peaks of the power spectrum obtained with the unconstrained ILC (K_{CMB}^2 unit). We expect, from Planck results, the spectrum to decrease around such values of the multipole moment. The best results are the (b) and (c) graphs.

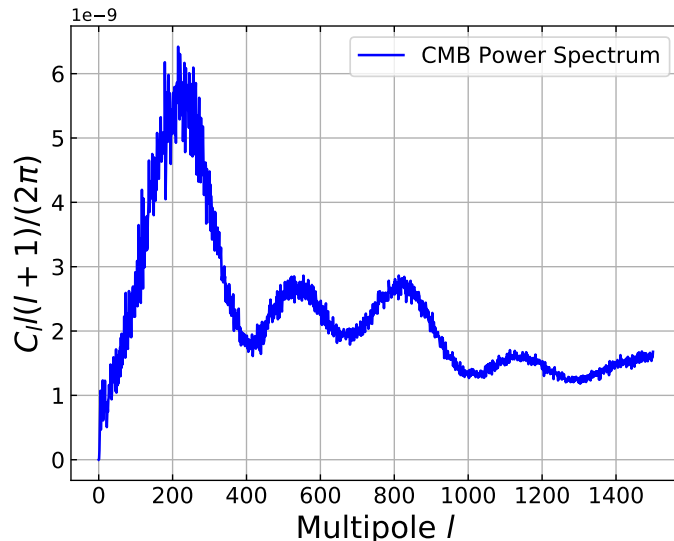


FIGURE 7 – Power spectrum (K_{CMB}^2 unit) obtained from a one-component ILC with a 20% mask.

5 Computing the power spectrum

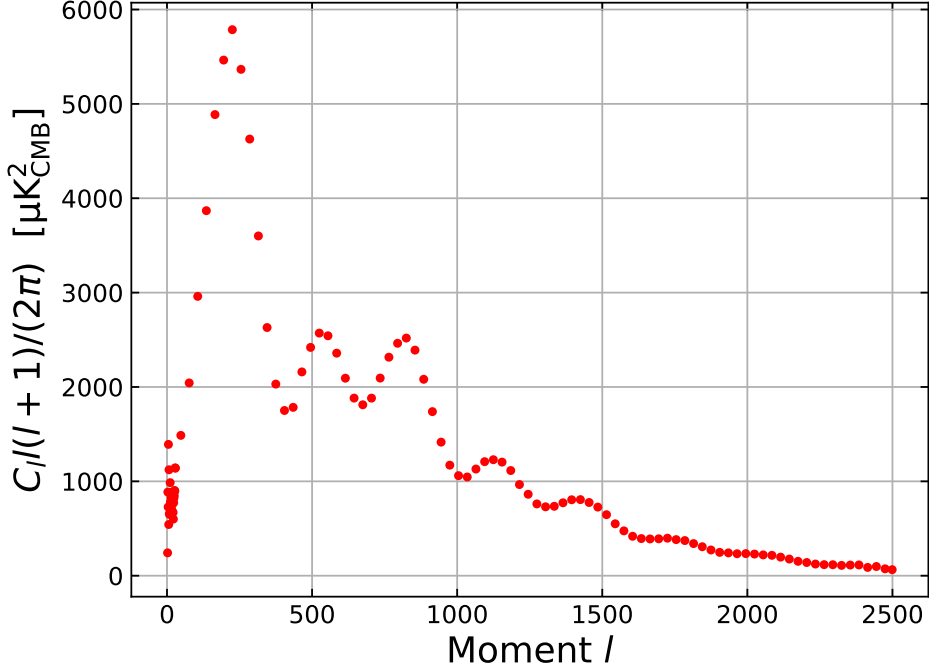


FIGURE 8 – Binned power spectrum from the Planck Collaboration

5.1 Power spectrum estimator

A way to check that our CMB map from the ILC is correct is to compare the obtained power spectrum with that of Planck. Indeed, if we infer that the fluctuations are Gaussian, then we can try to derive the variance of our CMB (the mean being null by hypothesis). This can be done either by computing the two points correlation function (in real space) or the power spectrum (in spherical harmonic space) which will both characterise the variance of the anisotropies of the CMB at different scales.

Starting from the two points correlation function (also called auto-correlation) which is defined as

$$\xi_{cc}(\Delta\theta) = \langle T(\mathbf{n}_1)T((\mathbf{n}_2)) \rangle \quad (9)$$

and which describes the correlation between two points $\mathbf{n}_1 = (\theta_1, \phi_1)$, $\mathbf{n}_2 = (\theta_2, \phi_2)$ on the sky separated by an angle $\Delta\theta$, we can compute a power spectrum $P(\Delta\theta)$, for which we can show that it corresponds to the Fourier transform of the two points correlation function, $\xi_{cc} \xrightarrow{\text{FT}} P$.

In the same way that we can develop a 1D function on Fourier space, we can develop (see [6] and [1]) the temperature variations on the sky (i.e. 2D) onto spherical harmonic space such as

$$T(\mathbf{n}) = \sum_{l=0}^{\infty} \sum_{m=-l}^l a_{l,m} Y_l^m(\mathbf{n}) \quad (10)$$

where $a_{l,m} \in \mathbb{C}$ are the coefficients^c and $Y_l^m = e^{im\phi} P_l^m(\cos\theta)$ the spherical harmonics, with P_l^m the Legendre polynomials.

We can notice that Eq.9 can be rewritten, based on Eq.10, as

$$\xi_{cc}(\Delta\theta) = \sum_{l_1, m_1} \sum_{l_2, m_2} \langle a_{l_1, m_1}^* a_{l_2, m_2} \rangle Y_{l_1}^{m_1}(\mathbf{n}_1) Y_{l_2}^{m_2}(\mathbf{n}_2) \quad (11)$$

We can then show that if we develop the $a_{l,m}$ coefficients onto the sphere (2D Fourier transform onto the sphere), the power spectrum $P(l)$ writes

c. By inverting Eq. 10 we find $a_{l,m} = \int_{4\pi} T(\mathbf{n}) Y_l^{m*}(\mathbf{n}) d\mathbf{n}$ (cf. [2])

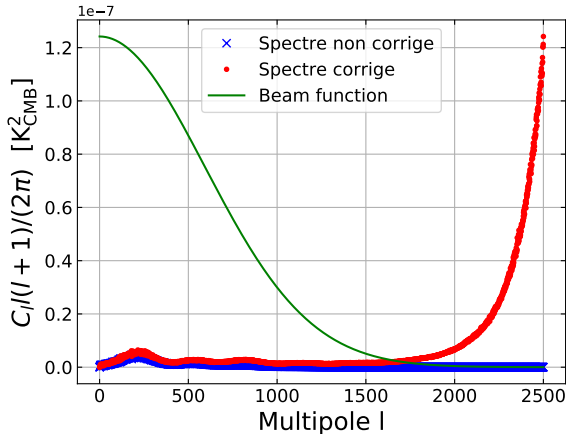
$$P(l) = \langle a_{l_1, m_1}^* a_{l_2, m_2} \rangle \delta_{l_1, l_2} \delta_{m_1, m_2} = \langle |a_{l, m}|^2 \rangle \quad (12)$$

where the means in Eq. 9 and Eq. 12 must be understood as on many realisations of the CMB (i.e. many Universes).

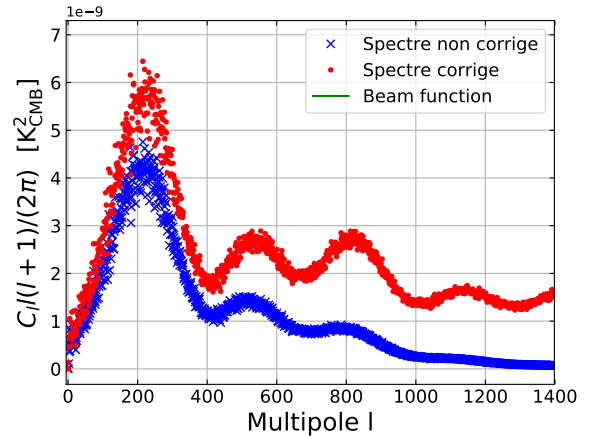
Since we suppose the fluctuations to be Gaussian, this means that on average the $a_{l, m}$ are supposed to be independent with respect to m . Thus, since $2l + 1$ $a_{l, m}$ are available at a fixed l , we can construct an estimator of $P(l)$, which we note C_l , by averaging the $a_{l, m}$ of our map for each value of l

$$C_l = \frac{1}{2l + 1} \sum_m |a_{l, m}^2| = \langle |a_{l, m}|^2 \rangle_m \quad (13)$$

where we are supposed to get $C_l \stackrel{l \gg 1}{\approx} P(l)$.



(a) Comparison of the spectra before and after applying the corrections.



(b) Zoom on the acoustic peaks of the two spectra.

FIGURE 9 – The spectra with (red curve) and without (blue curve) the corrections from Sec. 2.2 are showed on the figures (a) and (b). The uncorrected spectrum does have the first three peaks but the amplitudes are too weak. The corrected one does have the three acoustic peaks at the right amplitude, but it exponentially grows at high scales because of the beam function at the denominator in Eq. 21. The beam function is also plotted in figure (a) and its amplitude was arbitrarily fixed for better visibility.

5.2 Power spectrum : effect of the mask

We can try to compute the C_l given by Eq. 13. However, this formula is not directly usable as our ILC map is affected by many effects, among which the noise, the pixellisation, the PSF and the masks used to hide the galactic plane which is dominated by dust (see Section 4.1).

We will note \tilde{C}_l and $\tilde{a}_{l, m}$ the coefficients affected by the effects given above, and C_l , $a_{l, m}$ those of the CMB alone, which we are trying to recover.

We then model our final map according to the prescription given in Eq. 1, for which we need to add the effect of the mask onto the maps. If we note it W , the temperature on the map will be modified as

$$T(\mathbf{n}) \rightarrow T(\mathbf{n})W(\mathbf{n}) \quad (14)$$

We can then rewrite the coefficients $\tilde{a}_{l, m}$

$$\begin{aligned} \tilde{a}_{l, m} &= \int_{4\pi} T(\mathbf{n})W(\mathbf{n})Y_l^{m*}(\mathbf{n})d\mathbf{n} \\ &= \sum_{l_1, m_1} \alpha(l, m, l_1, m_1)a_{l_1, m_1} \end{aligned} \quad (15)$$

where $\alpha(l, m, l_1, m_1) = \int_{4\pi} W(\mathbf{n})Y_{l_1}^{m_1}(\mathbf{n})Y_l^{m*}(\mathbf{n})d\mathbf{n}$ are mixing coefficients. Hence, the mask has the effect to correlate the $a_{l, m}$ between each other, which implies that Eq. 13 is not correct any more.

To simplify the situation, we consider that the mask can be simply modelled as a constant factor $W(\mathbf{n}) = \sqrt{f}$ which is related to the fraction of the sky which was masked. This allows the $a_{l, m}$ to remain uncorrelated. Thus, Eq. 13 can be rewritten as

$$T(\mathbf{n}) \rightarrow \sqrt{f}T(\mathbf{n}) \quad (16)$$

5.3 Taking into account the noise

Apart from the effect of the mask (see Section 5.2), of the pixellisation and the PSF (see Section 2.2), a last effect on the \tilde{C}_l comes from the noise $N(\mathbf{n})$. Given that it is present since the measurement (statistical and instrumental noise), it has underwent the same effects due to the PSF and the mask. We therefore have

$$N(\mathbf{n}) \rightarrow \sqrt{f}N(\mathbf{n}) * \psi \quad (17)$$

5.4 Auto-spectrum

Now that we have taken into account all the aforementioned effects, we can look at how these will impact the $a_{l,m}$ coefficients. If we go into spherical harmonic space (SH) we have

$$T \xrightarrow{\text{SH}} a_{l,m} \quad N \xrightarrow{\text{SH}} a_{l,m}^N \quad M \xrightarrow{\text{SH}} \sqrt{f} \quad \psi \xrightarrow{\text{SH}} B_l \quad P \xrightarrow{\text{SH}} P_W \quad (18)$$

where B_l is the equivalent of the PSF into harmonic space (beam function) and P_W is the same for the pixellisation (window function). An example of the beam function which was used (the amplitude is arbitrary for visibility sake) is given in Fig. 9. Since the PSF is modelled by a Gaussian, by Fourier transform we recover a Gaussian on spherical harmonic space.

The convolutions becoming products, we get the following relations between the measured $\tilde{a}_{l,m}$ and the $a_{l,m}$ of the CMB

$$\tilde{a}_{l,m} = \sqrt{f}B_l(a_{l,m}P_W + a_{l,m}^N) \quad (19)$$

If we inject this equation in Eq. 13, we find

$$\tilde{C}_l = B_l^2 f \left(P_W^2 C_l + 2P_W \langle a_{l,m}^N a_{l,m}^* \rangle_m + C_l^N \right) \quad (20)$$

where $C_l^N = \langle |a_{l,m}^N|^2 \rangle_m$. The CMB and the noise being in principle uncorrelated, the cross-correlation term $\langle a_{l,m}^N a_{l,m}^* \rangle$ is 0. Hence, knowing the coefficients C_l^N of the noise, we are able to reconstruct the CMB coefficients as

$$C_l = \frac{1}{P_W^2} \left(\frac{\tilde{C}_l}{B_l^2 f} - C_l^N \right) \quad (21)$$

5.5 Noise coefficients

In order to reconstitute the CMB spectrum from Eq. 21, we need to find the noise coefficients C_l^N . To do so, we use the half-mission 1 and 2 maps (see Sec 1).

We model the noise by a white noise $b_k \sim W(0, \sigma)$, such that its statistical properties are the following

$$\mathbb{E}(b_k) = 0 \quad \text{Cov}(b_j, b_k) = \sigma^2 \delta_{jk} \quad (22)$$

If we perform the difference b_{diff} of two of its realisations $b_1, b_2 \sim W(0, \sigma)$, then we have

$$\mathbb{E}(b_{\text{diff}}) = 0 \quad (23)$$

$$\text{Var}(b_{\text{diff}}) = \mathbb{E}((b_1 - b_2)^2) = 2\sigma^2 \quad (24)$$

$$\mathbb{E}(b_{\text{diff},1} b_{\text{diff},2}) = \mathbb{E}((b_1 - b_2)(b_3 - b_4)) = 0 \quad (25)$$

from which we deduct that $(b_1 - b_2)/2 \sim W(0, \sigma)$. This property will be useful for deriving the C_l^N . Indeed, the two half-mission 1 and 2 maps, noted M_1^h, M_2^h , can be written as the sum of all the components such as CMB, SZ, etc, which we note D (convolved by the pixellisation and the PSF) and the noise b convolved by the PSF. If we compute the half difference between the two maps, we get a new map containing only a new realisation of the noise which we note b (up to a convolution)

$$\frac{M_1^h - M_2^h}{2} = \frac{(b_1 - b_2)}{2} * \psi = b * \psi \quad (26)$$

If we note m_l the C_l coefficients of our new map $(M_1^h - M_2^h)/2$, then we can construct an estimator of C_l^N as

$$\hat{C}_l^N = \frac{m_l}{B_l^2} \quad (27)$$

and we can reconstruct the CMB power spectrum by performing the transformation $C_l^N \rightarrow \hat{C}_l^N$ in Eq. 21.

We can ask ourselves if the whole aforementioned corrections do improve the final power spectrum. To answer this question, we can compare the obtained power spectrum with all the corrections with the one without any corrections (see Fig. 9).

In theory, we expect the CMB spectrum to decrease quite rapidly at high enough l . On the contrary, the noise power spectrum should remain constant with l as a consequence of the white noise hypothesis. Given that, in Eq. 13 and Eq. 27, the C_l of the CMB and that of the white noise are divided by the beam function, and given that the beam function is modelled by a Gaussian ($B_l \xrightarrow{l \gg 1} 0$), we expect the noise to exponentially increase at high enough values of l .

In practice, this is what we observe, and in spite of all the corrections we took into account concerning the noise in particular, we still have our C_l which diverge for high values of l . This is a sign that our methods, including the computation of the cross-spectrum (see Section 6), can still be improved.

6 Improving the power spectrum : cross-spectrum

The above procedure for correcting noise effects is in practice quite laborious and it is in our right to ask ourselves if there is not another technique much simpler at hand. This is what brought us to use the cross-spectrum rather than the auto-correlation correction.

In order to build it, we start back from Eq. 13, but this time we define our C_l estimator slightly differently

$$C_l^{\text{CP}} = \sum_m \left\langle a_{l,m}^{h_i} a_{l,m}^{h_i *} \right\rangle \quad (28)$$

where $a_{l,m}^{h_i}$ are the coefficients of half-mission i map. If we do not note the effects of the mask, the pixellisation and the PSF, which we will obviously have to take into account in the end, we can write the $a_{l,m}$ as the sum of those of the CMB with those of the noise (which we note $a_{l,m}^{N_i}$). Then we have

$$\begin{aligned} C_l^{\text{CP}} &= \sum_m \left(\left\langle a_{l,m} a_{l,m}^* \right\rangle + \left\langle a_{l,m} a_{l,m}^{N_2 *} \right\rangle + \left\langle a_{l,m}^{N_1} a_{l,m}^* \right\rangle + \left\langle a_{l,m}^{N_1} a_{l,m}^{N_2 *} \right\rangle \right) \\ &= \sum_m (\langle a_{l,m} a_{l,m}^* \rangle) \end{aligned} \quad (29)$$

Since we consider a white noise, two realisations are uncorrelated. In the same way, the CMB is uncorrelated to the noise as well, and thus only the first term in the above equation survives. Hence, we get an estimator which is not affected by the noise any more.

The power spectrum obtained via the cross-spectrum technique with a 20% mask is shown in Fig. 7. We find the same characteristics as for the auto-correlation technique (see Fig. 9b), namely the first three acoustic peaks and the very beginning of the damping zone of the spectrum. The damping is nonetheless slightly better, even though it still is too high compared to the CMB spectrum. Globally, the spectra via auto-correlation or cross-spectrum give identical results.

7 Comparison to the theoretical spectrum

7.1 General principle

Now that we have a spectrum which resembles that of Planck (see Fig. 8), our goal is to find the best fit to a theoretical CMB spectrum in order to deduct some cosmological parameters.

To do so, we used a Python wrapper of a Boltzmann type code called *CLASS* (the wrapper is named *Classy*, see [4] and [5]). This code computes a CMB power spectrum from a set of cosmological parameters (including inflation). The parameters we allowed ourselves to modify were as follows

- A , an amplitude parameter
- Ω_b , the baryon density parameter
- Ω_{CDM} , the dark matter density parameter

We can therefore model the theoretical spectrum as

$$g(l; A, \Omega_b, \Omega_{\text{CDM}}) = Af(l; \Omega_b, \Omega_{\text{CDM}}) \quad (30)$$

with f a function which is independent of the amplitude parameter and g the final theoretical spectrum.

7.2 Method for finding the amplitude

The simplest method to "find" the cosmological parameters is to set the values of the baryon and dark matter densities to that of Planck, $(\Omega_b h^2, \Omega_{\text{CDM}} h^2) = (0.022, 0.119)$, and then search the amplitude parameter which gives us a theoretical spectrum as close as possible.

By lack of time, we could not write a full functional minimisation procedure. Thus, we simply took, in first approximation, the maximum of our spectrum as the maximum we want for the theoretical spectrum and we allowed the amplitude to vary until it matched that of the spectrum.

After binning (10 points per bin) our spectrum, in such a way that it is smoothed out, and after having looking for the best value of the amplitude parameter, we obtained the final spectrum as well as a value of $A = 1.70 \cdot 10^{-8} K_{\text{CMB}}^2$. The result is plotted in Fig. 10.

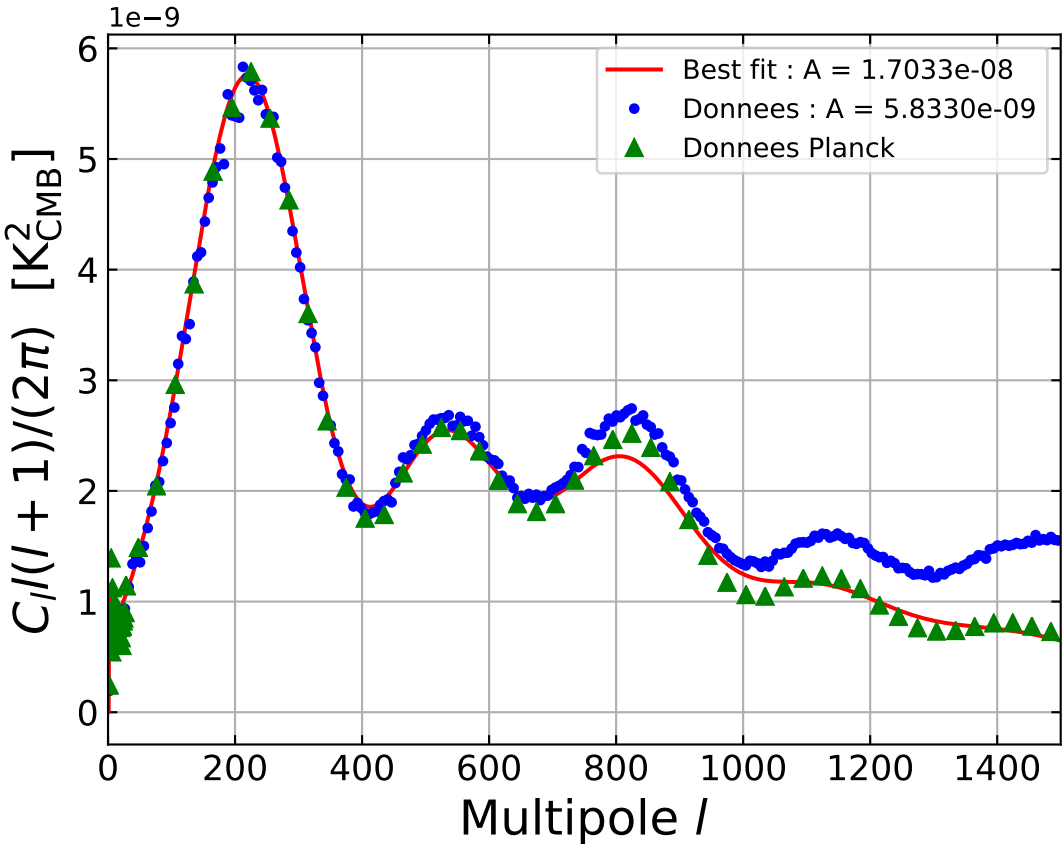


FIGURE 10 – Best fit for the parameter A with the density parameters fixed to the values of Planck. The data given by Planck (Fig. 8) are plotted as well for comparison. The value of A given in the legend for the data is different from the amplitude of the fit and correspond to the maximum of the first acoustic peak.

We can clearly see that the red curve, which represents the theoretical spectrum with the same maximum as the spectrum from the ILC (in blue), follows quite closely the green curve, which is the spectrum from Planck. It is highly possible that the cosmological parameters of our spectrum are different from those of Planck if we computed a proper fit, for instance with a least square fitting procedure. Nevertheless, if we focus on the first three acoustic peaks (up to $l \sim 1000$), we can still expect a least square procedure to give us reasonably close values of the density parameters. Obviously, there is still some work to be done to find, for instance, the cosmological model which our spectrum would best represent.

7.3 Potential future work

Many improvements can be made. First, we can check that the value obtained with the previous method is really the best-fit solution to our spectrum. To do so, we could perform a χ^2 test

$$\chi^2(A, \Omega_b, \Omega_{\text{CDM}}) = \sum_l \left(\frac{y_i - g(l; \Omega_b, \Omega_{\text{CDM}})}{\sigma_n} \right)^2 \quad (31)$$

where y is our power spectrum and g is the theoretical one.

In theory, given Eq 30, only Ω_b and Ω_{CDM} should be free parameters since the amplitude parameter A should be fixed by them. For instance, at fixed Ω_b and Ω_{CDM} , the best fit parameter for A will be the one which minimises the χ^2 , thus

$$\frac{d\chi^2}{dA} = -2 \sum_l \frac{f(l)}{\sigma_n} \left(\frac{y_i - Af(l)}{\sigma_n} \right) = 0 \quad (32)$$

This should in principle constrain the value of A . It is nevertheless necessary to be careful with the amplitude in the theoretical spectrum as, even if A were to be fixed, the other parameters would change the amplitude and the width of our peaks. We should therefore either evaluate A or directly perform the χ^2 test on both density parameters instead of fixing them and trying to find A .

8 Conclusion

During this project, we have used two Internal Linear Combination methods for extracting the CMB, the first without constraints on the other components, and the second by constraining the SZ signal. We have applied many masks with the aim to improve our CMB map, and we found that the 20% mask gave the best result. In order to make sure that our map did contain a CMB signal, we build its power spectrum. Two methods were used, the first one by auto-correlation and the other one by computing its cross-spectrum. Both give the typical characteristics of a CMB power spectrum, such as, for instance, the first three acoustic peaks with the right amplitude, up to a multipole moment of $l \approx 1500$. Finally, we tried to find the closest theoretical fit to our spectrum. We find that our power spectrum is coherent with a cosmogony Λ CDM with a null curvature and $(\Omega_b h^2, \Omega_{\text{CDM}} h^2) = (0.022, 0.119)$. However, more advanced methods than the ILC and the fitting procedure for the power spectrum which were used in this work are necessary to obtain a spectrum which gives correct results up to much more higher multipole moments (smaller angular scales).

Références

- [1] C. L. Bennett, M. Halpern, G. Hinshaw, N. Jarosik, et al. First-Year Wilkinson Microwave Anisotropy Probe (WMAP) Observations : Preliminary Maps and Basic Results. *The Astrophysical Journal Supplement Series*, 148 :1–27, Sep 2003.
- [2] E. Hivon and S. Galli. Cmb angular power spectra and their likelihoods :in theory and in (planck) practice. <http://www.cpt.univ-mrs.fr/~cosmo/EC2017/Presentations/Hivon-1.pdf>. Accessed : 2019-02-22.
- [3] G. Hurier, J. F. Macías-Pérez, and S. Hildebrandt. MILCA, a modified internal linear combination algorithm to extract astrophysical emissions from multifrequency sky maps. , 558 :A118, Oct 2013.
- [4] Lesgourg. CLASS code webpage. <http://class-code.net/>.
- [5] Lesgourg. Classy GitHub webpage. https://github.com/lesgourg/class_public/wiki/Python-wrapper.
- [6] Cole Miller. Astr 422, cosmology lecture 21. <https://www.astro.umd.edu/~miller/teaching/astr422/lecture21.pdf>. Accessed : 2019-02-22.
- [7] Planck Collaboration, P. A. R. Ade, N. Aghanim, C. Armitage-Caplan, M. Arnaud, et al. Planck 2013 results. IX. HFI spectral response. , 571 :A9, Nov 2014.
- [8] Planck Collaboration, P. A. R. Ade, N. Aghanim, C. Armitage-Caplan, M. Arnaud, et al. Planck 2013 results. VII. HFI time response and beams. , 571 :A7, Nov 2014.
- [9] Mathieu Remazeilles, Jacques Delabrouille, and Jean-François Cardoso. CMB and SZ effect separation with constrained Internal Linear Combinations. , 410 :2481–2487, Feb 2011.